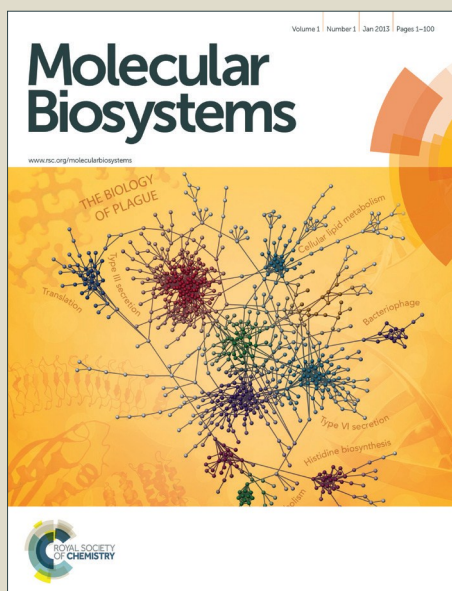


# Molecular BioSystems

Accepted Manuscript



This is an *Accepted Manuscript*, which has been through the Royal Society of Chemistry peer review process and has been accepted for publication.

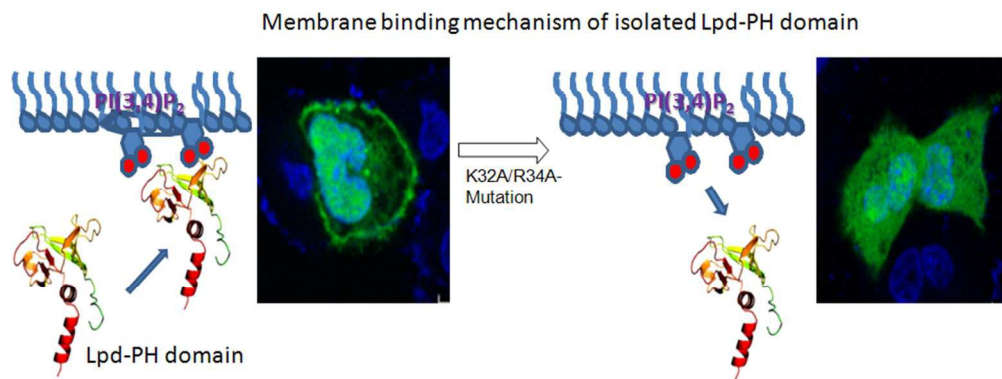
*Accepted Manuscripts* are published online shortly after acceptance, before technical editing, formatting and proof reading. Using this free service, authors can make their results available to the community, in citable form, before we publish the edited article. We will replace this *Accepted Manuscript* with the edited and formatted *Advance Article* as soon as it is available.

You can find more information about *Accepted Manuscripts* in the [Information for Authors](#).

Please note that technical editing may introduce minor changes to the text and/or graphics, which may alter content. The journal's standard [Terms & Conditions](#) and the [Ethical guidelines](#) still apply. In no event shall the Royal Society of Chemistry be held responsible for any errors or omissions in this *Accepted Manuscript* or any consequences arising from the use of any information it contains.



[www.rsc.org/molecularbiosystems](http://www.rsc.org/molecularbiosystems)



335x129mm (72 x 72 DPI)

# Mechanistic Insights into the Phosphatidylinositols Binding Properties of Pleckstrin Homology Domain of Lamellipodin

Sukhamoy Gorai,<sup>a</sup> Debasish Paul,<sup>b</sup> Nandan Haloi,<sup>a</sup> Rituparna Borah,<sup>a</sup> Manas Kumar Santra,<sup>\*b</sup> and Debasish Manna<sup>\*a</sup>

<sup>a</sup>*Department of Chemistry, Indian Institute of Technology Guwahati, Assam 781039, India.*

<sup>b</sup>*National Center for Cell Science, Pune 411007, Maharashtra, India*

## Abstract

Lamellipodin (Lpd) protein plays an important role in the formation of lamellipodial protrusion which is crucial in actin dynamics, cell polarity and motility. Lpd promotes actin polymerization with the help of members of Ena/VASP family of actin regulators and tethering them to actin filaments. It is well documented that Lpd protein interacts with the membrane containing phosphatidylinositols through its pleckstrin homology (PH) domain and regulates several cellular functions and cell migration. However, the molecular mechanism that underlies how the PH domain of Lpd specifically gets recruited to phosphatidylinositols remains unclear. To understand their interaction properties, we quantitatively determined the binding parameters of Lpd-PH domain employing a number of biophysical studies including surface plasmon resonance (SPR), fluorescence resonance energy transfer (FRET)-based competitive binding

---

assay and monolayer penetration measurements. Our studies showed that Lpd-PH domain strongly interacts with PI(3,4)P<sub>2</sub> containing liposome without any membrane penetration. Mutational studies demonstrate that the presence of cationic residues within the phosphatidylinositol (PIP) binding site of Lpd-PH domain is essential in membrane binding. The translocation patterns of Lpd-PH domain and mutants in platelet-derived growth factor (PDGF) stimulated A549 cells are in good agreement with our *in vitro* binding measurements. Overall, these studies demonstrate an insight into how Lpd-PH domain regulates cellular signals in PI(3,4)P<sub>2</sub> dependent manner.

## Introduction

Perturbation of actin-dependent cell migration and adhesion is associated with malignant cell metastasis and other diseases. Lamellipodin (Lpd) plays a crucial role in actin-dependent cell migration and adhesion.<sup>1-5</sup> Cell motility and actin dynamics have been found to be associated with a group of adapter signaling proteins designated as MRL family (based on family members MIG-10/RIAM/Lpd), demonstrated to promote lamellipodia protrusion in fibroblasts.<sup>3-10</sup> These proteins are recognized as a key convergence point that links upstream signaling with actin dynamics. It is well documented that Lpd acts as a junction point between upstream signaling pathways and cytoskeletal remodeling through its phosphatidylinositols (PIP) binding pleckstrin homology (PH) domain and Ras-superfamily proteins binding Ras associating (RA) domain at the plasma membrane.<sup>2, 3</sup> It is highly expressed in nerve, heart, brain, and ovary.<sup>3</sup> Lpd over expression augments lamellipodial projection speed, a consequence detected when Ena/vasodilator-stimulated phosphoproteins (VASP) are over expressed or stimulated at the plasma membrane. Ena/ VASP proteins also play a crucial role in cytoskeleton rearrangement including

migration, adhesion, cell–cell interaction and shape change. Lpd directly interacts with Ena/VASP via clusters of putative EVH1 binding site and recruits at lamellipodia and the tips of the filopodia. Pathogens like vaccinia and enteropathogenic *E. coli* (EPEC) use Ena/VASP molecules and Lpd as a tool to move them throughout inter or intra cells.<sup>11</sup> Reduced lamellipodia formation efficiency was observed in Lpd knock-down cells but not in Ena/Vasp knock-down cells. This suggests the importance of Lpd in actin-cytoskeleton dynamics. Like other FP4 motif containing proteins, Lpd also localize and recruits Ena/VASP proteins to the focal adhesion sites. Although, over-expression of Lpd is dependent on Ena/VASP proteins but functional localization at the leading edge is completely independent.<sup>4, 12-16</sup> Lpd is also considered as a potent therapeutic target for the treatment of cocaine abuse and toxicity for its catalytic activity of butylcholinesterase.<sup>17-19</sup> The Lpd is reported to localize at the ruffles in phosphoinositide-3-kinase (PI3K) activated cells.<sup>3</sup> The activation of PI3K in response to growth factors and insulin stimulation leads to the generation of phosphatidylinositol 3-phosphate PI(3)P, phosphatidylinositol 3,4,5-trisphosphate [PI(3,4,5)P<sub>3</sub>] and phosphatidylinositol 3,4-bisphosphate [PI(3,4)P<sub>2</sub>].<sup>20</sup> These PIPs also play an important role in cell motility, signal transduction, membrane trafficking and cytoskeletal dynamics.<sup>10, 21</sup>

Crystal structures of Lpd demonstrate the similar structural building block as MRL protein family. Like the analogues protein RIAM, Lpd also contain highly charged N-terminus RA, PH, coiled-coil region and a number of poly-proline motifs.<sup>4, 6, 9</sup> Furthermore, the C-terminus of Lpd consist proline rich eight possible SH3 binding sites followed by three proline and six EVH1 binding sites. In mammalian system, RA and PH domains cooperatively regulates in both Ras-GTPase signaling and membrane translocation via RA and PH domain, respectively.<sup>7</sup> Further structural analyses also revealed that Lpd oligomerizes through

intermolecular coil-coil interaction. This interaction is important for the recruit of Ena/VASP proteins; thereby leading to the binding of actin-filaments forming bundles.<sup>5,6</sup>

Structural analysis showed that like other PH domains, the Lpd-PH domain also contain a conserved structure consisting of seven  $\beta$ -sheets strands with variable loops, followed by one  $\alpha$ -helix.<sup>11,22</sup> Characteristically, PH domains exhibit high to-low specificity for the PIPs containing membrane. Sequence alignment and structure analysis revealed that Lpd-PH domain has several positively charged residues on its membrane binding surface, which might be primarily responsible for its interaction with the anionic lipids like PIPs. Recent studies demonstrated that the PH domain of Lpd protein moderately interacts with the PI(3,4)P<sub>2</sub> and EGFP-fused Lpd PH domain localized at the ruffles in PDGF-stimulated cells.<sup>2</sup> However, PIP-binding specificities were not measured quantitatively and PIP-dependent membrane binding mechanism is also not known.

In the current study we present a thorough understanding of the PIP-binding mechanism and PIP-dependent cellular localization of the Lpd-PH domain. To elucidate the mechanism by which PIP lipids recruit the membrane effectors Lpd protein, we successfully performed a series of biophysical experiments to determine the binding affinity and specificity. Fluorescence resonance energy transfer (FRET) analysis and surface plasmon resonance (SPR) measurements showed that Lpd-PH domain strongly interact with the PI(3,4)P<sub>2</sub> lipid containing membranes but monolayer penetration measurements showed its inability to significantly penetrate into the membrane even in the presence of PI(3,4)P<sub>2</sub> lipid. However cellular studies showed that EGFP-fused Lpd PH domain localize at the plasma membrane in PDGF-stimulated A549 cells. Overall, our combined theoretical and experimental analyses showed that positively charged residues

present at the membrane binding surface of Lpd PH domain predominantly regulate the PI(3,4)P<sub>2</sub>-dependent membrane binding properties of Lpd protein.

## Results

**Quantitative *in vitro* analyses of phosphatidylinositol specificities of Lpd-PH Domain**—PH domains are one the common membrane binding modules with varying (weak to strong) affinities for PIP lipids and involved in regulation of PIP level in different cellular compartments. PIP-dependent membrane binding of the PH domains serves as a common membrane translocalization function of the host proteins.<sup>23, 24</sup> RA-PH domain containing proteins like Grb and others also get anchored into the membrane in a PIP-dependent manner and facilitate the interactions of RA domain with Ras GTPases, which augments the signaling events.<sup>5, 7</sup> Few studies already mentioned that Lpd-PH domain weakly interacts with PIPs. However, conflicting results have been reported regarding its PIP-specificities and binding affinities. Using various fluorescently labeled PIPs in a fluorescence-polarization assay Professor Jinhua Wu and coworkers recently reported that Lpd-cc-RA-PH domain have only lower affinities for PI(5)P, PI(3,4)P<sub>2</sub>, PI(4,5)P<sub>2</sub> and PI(3,4,5)P<sub>3</sub> lipids ( $K_d$  in the range of 29-69  $\mu$ M).<sup>6</sup> Whereas Frank B. Gertler and coworkers performed protein-lipid overlay assay and showed that Lpd-PH domain specifically interacts with PI(3,4)P<sub>2</sub>.<sup>3</sup> In this regard, we quantitatively measured the PIP binding affinities and specificity of the isolated Lpd-PH domain using real-time surface plasmon resonance (SPR) measurement and fluorescence resonance energy transfer (FRET)-based competitive binding analysis under liposomal environment.

**Fluorescence resonance energy transfer-based competitive binding assay identifies PI(3,4)P<sub>2</sub> specificity of Lpd-PH domain**— To determine the PIP-binding affinities and specificity of Lpd-PH domain, we employed FRET-based competitive binding assay under the liposomal environment (PC/PE/PS/dPE/PIP (57:19:20:1:3)).<sup>25</sup> First Lpd-PH domain was equilibrated with liposomes and FRET signal was collected and then this lipid-protein interaction was perturbed by using competitive inhibitor, phytic acid (IP<sub>6</sub>) in a concentration dependent manner. The decrease in FRET signal at 505 nm was monitored to measure the apparent inhibitory constant [ $K_I(IP_6)_{app}$ ] values. Surface exposed Trp-residue (W22, W31) of the Lpd-PH domain act as the FRET donor, and a low density of membrane-embedded, dansyl-PE (dPE) lipid serve as the acceptors. Figure 1A illustrates representative isotherms of protein-to-membrane FRET-assay. Calculated  $K_I(IP_6)_{app}$  values for different PIP containing liposomes are listed in Table 1.

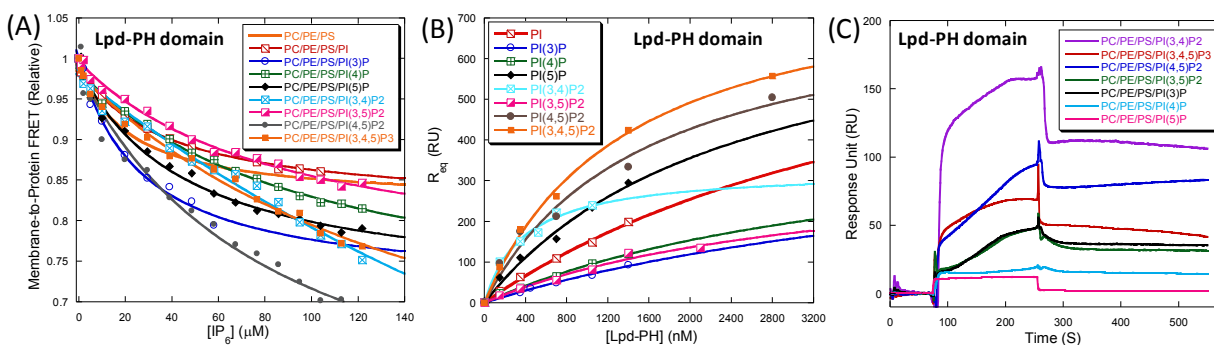


**Figure 1: Representative binding isotherms of Lpd-PH domain under liposomal environment.** Competitive displacement assay for Lpd-PH domain (1 μM) bound to PC/PE/PS (60:20:20) and PC/PE/PS/PIP (57:20:20:3) liposomes. The bound complex was titrated with the IP<sub>6</sub> as competitive inhibitor (A). Representative equilibrium SPR sensorgrams for Lpd-PH domain interacting with the PC/PE/PS/PIP (57:20:20:3) liposomes immobilized on L1 sensor chip at 25 °C. PIPs binding isotherms were generated from the R<sub>eq</sub> values after 500 sec in a

concentration dependent manner (B). Representative kinetics SPR sensograms of Lpd-PH domain interacting with the PC/PE/PS/PIP (57:20:20:3) liposomes at 25 °C (C). FRET measurements were performed in 20 mM Tris buffer at pH 7.4 containing 160 mM NaCl. 20 mM HEPES buffer at pH 7.4 containing 160 mM KCl, was used for all SPR measurements. The SPR sensorgrams are shown after background correction for binding to the control surface coated with PC/PE/PS (60:20:20) liposome and BSA (40  $\mu$ L of 0.1 mg/mL in the running buffer). Flow rate was kept at 10 and 30  $\mu$ L/min for equilibrium and kinetic SPR analyses, respectively. Protein concentrations were varied for SPR analysis.

***Surface plasmon resonance analysis identifies PI(3,4)P<sub>2</sub> specificity of Lpd-PH domain***— For further understanding of the Lpd-PH domain interaction patterns with different PIPs and measurements of quantitative binding parameters, we also performed real-time SPR analysis using PIP-containing liposomes (PC/PE/PS/PIP<sub>x</sub> (57:20:20:3)).<sup>23, 26</sup> The binding PIP binding affinities were calculated using both equilibrium- and kinetic-SPR analyses. For equilibrium-SPR measurements different concentrations of wild type (WT)-Lpd-PH domain was passed over the liposome-coated L1 sensor chip at a flow rate of 10  $\mu$ L/min and real-time measurement of association phase was monitored for longer time (for 500 sec). Figure 1B describes representative binding isotherms of equilibrium-SPR measurements. Protein concentration dependent maximum SPR responses (after 500 sec) are plotted to calculate the binding affinities ( $K_{d1}$ ) and are listed in Table 1. Figure S1 illustrates representative SPR sensorgrams for the binding of Lpd-PH domain to PC/PE/PS/PI(3,4)P<sub>2</sub> (57:20:20:3) liposomes. We also performed kinetic-SPR analyses using PIP-containing liposomes (PC/PE/PS/PIP<sub>x</sub> (57:20:20:3)). For kinetic-SPR analyses different concentrations of WT-Lpd-PH domain was passed over the liposome-

coated L1 sensor chip at a flow rate of 30  $\mu\text{L}/\text{min}$  and real-time measurement of both association and dissociation phase was monitored (Figure 1C). Calculated binding affinities ( $K_{d2}$ ) and are listed in Table 1.

Calculated  $K_{d1}$  and  $K_{d2}$  values obtained from the SPR analyses are in good agreement with the  $K_{I(\text{IP}_6)_{\text{app}}}$  values measured from the competitive-FRET analyses. The binding parameters showed that the WT-Lpd-PH domain have sufficiently stronger binding affinity for PI(3,4)P<sub>2</sub> lipid. The  $K_{d1}$  and  $K_{d2}$  values of WT-Lpd-PH domain for PI(3,4)P<sub>2</sub> lipid are 388 nM and  $3.80 \times 10^{-9}$  M, where, the  $K_{I(\text{IP}_6)_{\text{app}}}$  value for PI(3,4)P<sub>2</sub> lipid is 460  $\mu\text{M}$ . However, the binding affinity of Lpd-PH domain for PI(3,4)P<sub>2</sub> is much weaker than the Tapp1-PH domain under the similar experimental conditions. The  $K_{d1}$  and  $K_{d2}$  values for Tapp1-PH domain under similar experimental conditions were 82 nM and  $1.31 \times 10^{-9}$  M, respectively (Table S1). Tapp1-PH

**Table 1.** Binding parameters of Lpd-PH domain interaction with PC/PE/PS/PIP (57:20:20:3) liposomes were determined membrane-to-protein FRET analysis and SPR analyses<sup>a</sup>

Liposome	Lpd-PH WT		
	$K_{I(\text{IP}_6)_{\text{app}}}$ ( $\mu\text{M}$ )	$K_{d1}$ (nM)	$K_{d2}$ (M)
PC/PE/PI	37 $\pm$ 8	4886 $\pm$ 141	-
PC/PE/PS/PI(3)P	74 $\pm$ 7	5716 $\pm$ 365	-
PC/PE/PS/PI(4)P	101 $\pm$ 14	4035 $\pm$ 169	-
PC/PE/PS/PI(5)P	46 $\pm$ 7	2452 $\pm$ 115	-
PC/PE/PS/ PI(3,4)P <sub>2</sub>	460 $\pm$ 32	388 $\pm$ 26	$3.80 \times 10^{-9}$
PC/PE/PS/ PI(3,5)P <sub>2</sub>	88 $\pm$ 14	3309 $\pm$ 152	-
PC/PE/PS/ PI(4,5)P <sub>2</sub>	85 $\pm$ 23	1557 $\pm$ 148	$2.08 \times 10^{-8}$
PC/PE/PS/ PI(3,4,5)P <sub>3</sub>	171 $\pm$ 20	1390 $\pm$ 143	$1.16 \times 10^{-8}$

<sup>a</sup>All FRET measurements were performed in 20 mM Tris buffer at pH 7.4 containing 160 mM NaCl. IP<sub>6</sub> was used as inhibitor of membrane-to-protein interactions. Protein, 1  $\mu\text{M}$  was used for FRET analysis. All SPR measurements were performed in 20 mM HEPES buffer at pH 7.4 containing 160 mM KCl at 25 °C. Protein concentrations were varied for SPR analysis. Values represent the mean  $\pm$  SD from triplicate measurements.  $K_{d1}$  values were calculated by nonlinear least squares fit analysis of the isotherm using  $R_{\text{eq}} = R_{\text{max}}/(1 + K_{d1}/P)$ . All SPR sensorgrams are shown after background correction for binding to the control surface coated with PC/PE/PS (60:20:20) liposome. Flow rate was kept at 10 and 30  $\mu\text{L}/\text{min}$  for equilibrium and kinetic SPR analyses, respectively. Values represent the mean  $\pm$  SD from triplicate measurements.

domain is considered as a cellular marker for PI(3,4)P<sub>2</sub> lipid.<sup>31</sup> The Lpd-PH domain also exhibited a moderate binding affinities for PI(3,4,5)P<sub>3</sub> (~3 fold less), PI(4,5)P<sub>2</sub> (~5 fold less) lipids but weaker affinities for other PIPs. However, WT-Lpd-PH showed dissimilar kinetic patterns. Rate constants ( $k_a$  and  $k_d$ ) could not be straightforwardly calculated and directly compared among the PIPs, because the sensograms for kinetic-SPR analyses followed complex patterns of either one-step or two-step 1:1 binding models. The sensograms of WT-Lpd-PH binding to the PI(3,4)P<sub>2</sub>, PI(4,5)P<sub>2</sub> and PI(3,4,5)P<sub>3</sub> lipids could be fitted using one-step 1:1 binding model. For this purpose, only the qualitative comparison of kinetic patterns was made for other PIP containing liposomes (Figure 1C). Similarly, we also measured the PIP-binding properties of Lpd-RA-PH domain. The  $K_{I(IP_6)_{app}}$  values showed that like isolated PH domain, RA-PH domain also preferentially bind with the PI(3,4)P<sub>2</sub> containing liposome (805  $\mu$ M) but with 1.75-fold stronger affinity (Table S2). Our dynamic light scattering (DLS) measurements with the isolated Lpd-PH domain suggest that there was no dimerization or higher-order oligomerization formation of the protein (concentration upto 6  $\mu$ M) molecules under the experimental conditions (Figure S2). Therefore, our FRET and SPR analyses clearly showed that Lpd-PH domain have higher specificity for PI(3,4)P<sub>2</sub> over other PIPs (Table 1). Collectively these quantitative binding parameters re-assess the PIP specificity and affinities of isolated Lpd-PH domain and provide a new insight into how Lpd-PH domain would respond to PI(3,4)P<sub>2</sub> formation more effectively than other PIPs under different cellular conditions.

***Identification of the PIP-binding site of the Lpd-PH Domain by mutation analyses:*** To identify the amino acids residues primarily involved in interactions with the PI(3,4)P<sub>2</sub> lipid, we analyzed the crystal structure of the Lpd-PH domain (4GN1) and amino acid sequences of the homologous

PH domain (Figure 2).<sup>6</sup> Surface electrostatic potential distribution calculation showed a cationic groove near the

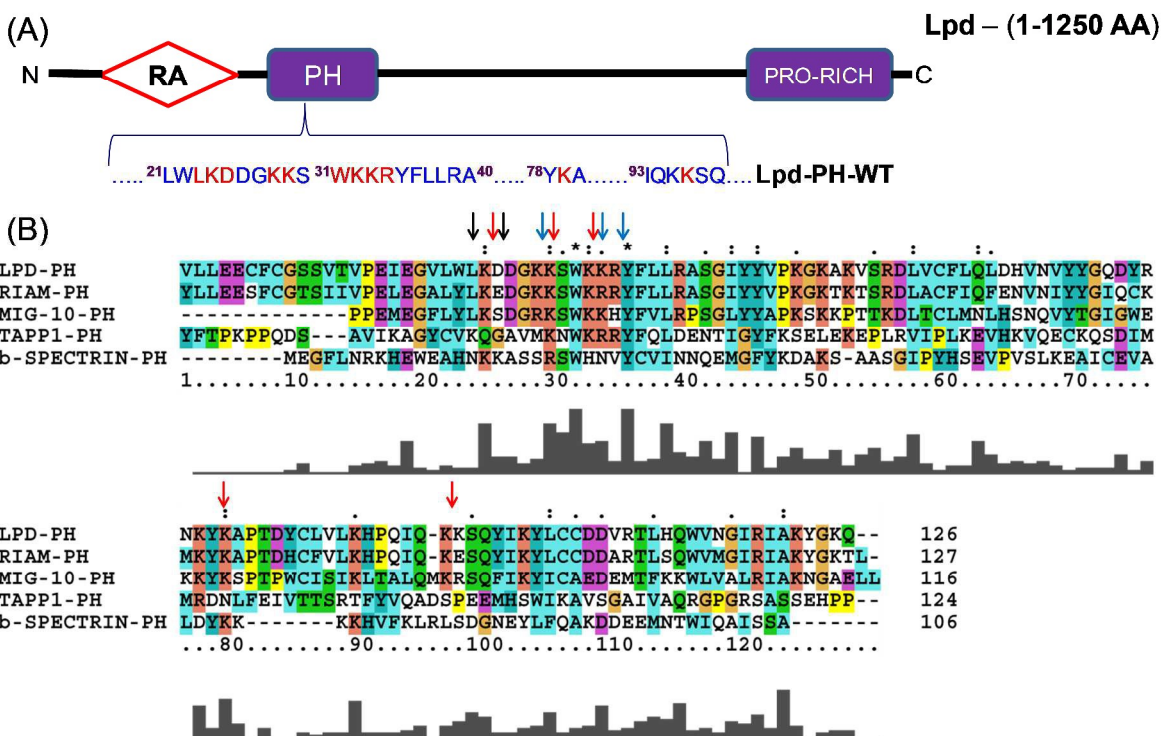


**Figure 2:** A schematic representation of the full-length Lpd protein (A). Amino-acid sequence alignment of the isolated PH domains of MRL protein family along with Tapp1 and  $\beta$ -spectrin are shown using Clustal-X program (B). Arrow indicates positions of the mutation.

putative membrane binding surface. Interestingly, we identified a cationic groove comprising K24, K29, K79 and K96 as a non-canonical PIP binding site like  $\beta$ -spectrin-PH domain. Whereas another cationic groove comprising K28, K32 and R34 present at the regular canonical PIP-binding site of PH domains (Figure 3). Therefore, Lpd-PH domain may interact with the PIP through the non-canonical binding site like  $\beta$ -spectrin-PH domain, or through regular canonical

binding mode (Figure 3). Detailed structural analysis of Lpd-PH domain and  $\beta$ -spectrin-PH domain (1BTN) showed that L23 and D25 residues could prevent the PIP-head groups to interact with the Lpd-PH domain through its canonical binding site.<sup>27</sup> To get initial information about the probable PIP-binding site, we performed molecular docking analyses with both short chain PI(3,4)P<sub>2</sub> lipid and Ins(1,3,4)P<sub>3</sub> molecule. However, the model structures revealed that both PI(3,4)P<sub>2</sub> and Ins(1,3,4)P<sub>3</sub> have almost no preference for either canonical or

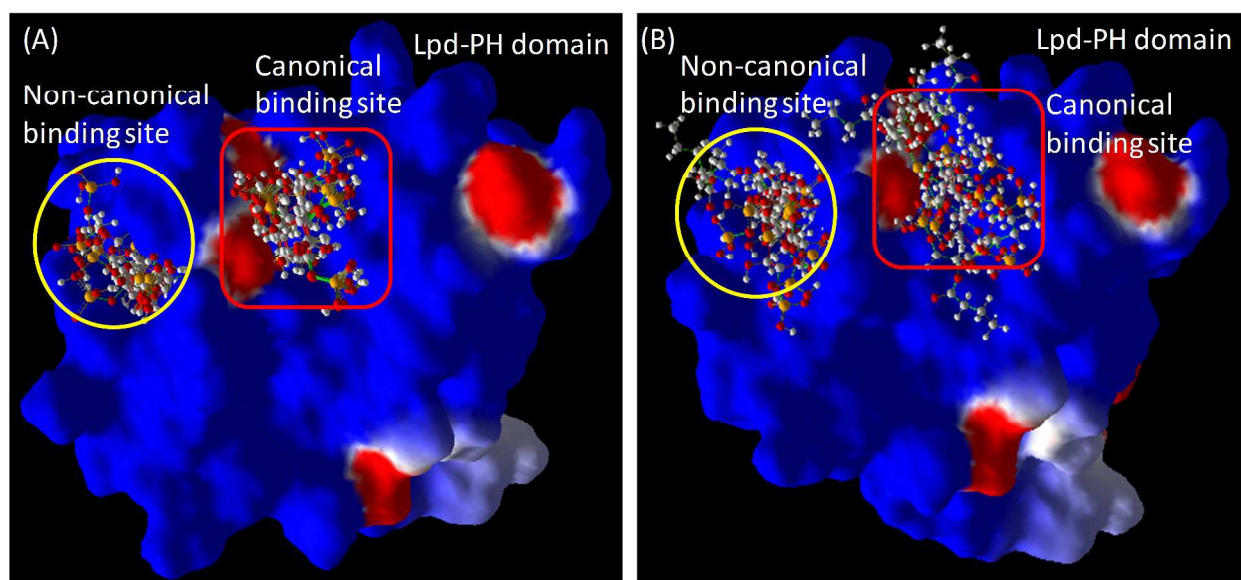


**Figure 3: Model structure of ligand-bound Lpd-PH domain based on the crystal structure of mouse LPD-RAPH domain (4GN1).** Surface representations of model structures of Lpd-PH domain docked with Ins(1,3,4)P<sub>3</sub> and PI(3,4)P<sub>2</sub> ligands. Probable PIP binding sites are shown in circles (yellow color) and squares (red color) and labeled. Red and blue colors indicate negative and positive potentials, respectively calculated by PyMol software. Ins(1,3,4)P<sub>3</sub> and PI(3,4)P<sub>2</sub> are shown in ball-stick representations. The modeled structures were generated using Molegro Virtual Docker, version 4.3.0.

non-canonical PIP-binding site. In this regards, we prepared a set of mutants for both the binding sites based on the crystal structure of the Lpd-PH domain. Cationic residues were mutated to Ala-residue either individually or in combination and their PI(3,4)P<sub>2</sub> binding affinities were measured by competitive-FRET or SPR analyses under the similar experimental conditions. Calculated binding parameters of the mutants are summarized in Table 2 and 3. The  $K_d$  values obtained from the SPR analyses show that single mutants K24A, K28A, R79A separately showed 2.3-7 fold lower binding affinities for PI(3,4)P<sub>2</sub> lipid than WT-PH domain of Lpd

**Table 2:** Apparent inhibitory constants [ $K_i(\text{IP}_6)_{\text{app}}$ ] for Lpd-PH domain and mutants binding to PC/PE/PS/PI(3,4)P<sub>2</sub> (57:20:20:3) liposomes were determined from protein-to-membrane FRET analysis<sup>a</sup>

Protein	$K_i(\text{IP}_6)_{\text{app}}$ ( $\mu\text{M}$ )	Fold change
PH (WT)	460 $\pm$ 32	1
PH-K24A	307 $\pm$ 20	1.5
PH-K29A/W31A	242 $\pm$ 31	1.7
PH-K79A	157 $\pm$ 23	2.9
PH-K96A	183 $\pm$ 12	2.5
PH-K28A	120 $\pm$ 27	3.8
PH-K32A/R34A	71 $\pm$ 12	5.7
PH-L23R/D25G	539 $\pm$ 39	-
PH-L23R/D25G/K29A	312 $\pm$ 25	-

<sup>a</sup>All measurements were performed in 20 mM Tris buffer at pH 7.4 containing 160 mM NaCl. IP<sub>6</sub> was used as inhibitor of membrane-to-protein interactions. Protein, 1  $\mu\text{M}$ . Values represent the mean  $\pm$  SD from triplicate measurements.

protein. Whereas, double mutants K29/W31A and K32/R34A showed 2- and 24-fold lower binding affinities for PI(3,4)P<sub>2</sub> lipid, respectively that WT-PH domain. Similarly FRET-analyses also showed that double mutants K29/W31A and K32/R34A have 1.7- and 5.7-fold lower binding affinities for PI(3,4)P<sub>2</sub> lipid, respectively, than WT-PH domain. Other mutants show moderately reduced affinity for PC/PE/PI(3,4)P<sub>2</sub> liposomes. Molecular dynamics (MD)

simulation studies (performed for 10 ns) of the docked structures of the isolated Lpd-PH domain and K32/R34A mutant with Ins(1,3,4)P<sub>3</sub> also suggest that K32 and R34 are crucial for lipid binding (Figure S3). Ins(1,3,4)P<sub>3</sub> is the only headgroup of PI(3,4)P<sub>2</sub> lipid and used as model for MD simulation studies. The change in root-mean-square deviation (RMSD) for both the structure showed that Lpd-PH domain forms a dynamically-stable complex with Ins(1,3,4)P<sub>3</sub> (after 1.5 ns) than that for Lpd-PH-K32A/R34A mutant. MD simulation also shows that Lpd-PH domain forms strong hydrogen-bond with K32, R34A residues and also interacts with D26, Y44 and K83 residues. Additionally, our MD simulation also showed the deviation of Ins(1,3,4)P<sub>3</sub> from the original binding site, which is in accordance with our experimental results. Collectively, these mutational data indicate that both K32 and R34 residues strongly interact with the headgroup of PI(3,4)P<sub>2</sub> lipid and cationic K28, K32 and R34 constitute the PIP-binding site of the Lpd-PH domain.

**Table 3:** Membrane binding affinity ( $K_{d2}$ ) measurements by kinetic SPR analyses.

Protein	$k_a$ (M <sup>-1</sup> S <sup>-1</sup> )	$k_d$ (S <sup>-1</sup> )	$K_{d2}$ (M)	Fold change
PH (WT)	$4.30 \times 10^4$	$1.62 \times 10^{-4}$	$3.80 \times 10^{-9}$	1
PH-K24A	$1.85 \times 10^4$	$1.62 \times 10^{-4}$	$8.76 \times 10^{-9}$	2.3
PH-K29A/W31A	$1.17 \times 10^4$	$4.13 \times 10^{-4}$	$3.53 \times 10^{-8}$	8.7
PH-K79A	$2.27 \times 10^4$	$6.11 \times 10^{-4}$	$2.69 \times 10^{-8}$	7
PH-K96A	$3.58 \times 10^4$	$4.84 \times 10^{-5}$	$1.35 \times 10^{-9}$	2.8
PH-K28A	$4.30 \times 10^4$	$7.30 \times 10^{-4}$	$1.70 \times 10^{-8}$	4.5
PH-K32A/R34A	$4.70 \times 10^3$	$4.40 \times 10^{-4}$	$9.30 \times 10^{-8}$	24.5
PH-L23R/D25G	$1.15 \times 10^4$	$2.17 \times 10^{-5}$	$1.89 \times 10^{-9}$	-
PH-L23R/D25G/K29A	$2.03 \times 10^4$	$2.14 \times 10^{-4}$	$1.06 \times 10^{-8}$	-

<sup>a</sup>All measurements were performed in 20 mM HEPES buffer at pH 7.4 containing 160 mM KCl.

***Membrane penetration ability of the Lpd-PH domain using monolayer and SPR analyses—***

PIP-dependent membrane interactions of the FYVE, PH, PX, and ENTH-domains are associated with frequent membrane penetration due to adjustment in electrostatic surface potential and/or

local conformational changes of the proteins. However, most of the reported PH domains have no significant membrane penetration ability.<sup>23, 28-30</sup> To date, only the PLC $\delta$ 1, Tapp1 and Dapp1-PH domains have been reported to have a significant membrane penetrating activity.<sup>31-33</sup> Cellular studies reported that PIP-binding of the PH domain and protein binding of the RA at the plasma membrane plays a significant role in Lpd-dependent upstream cell signaling and cytoskeleton remodeling.<sup>7, 34</sup> However, it is unclear whether PIP-dependent membrane binding of the PH or RA-PH domains of Lpd protein is supported by membrane bilayer penetration. Therefore, to understand the membrane penetration ability of Lpd-PH, we measured the surface pressure of the above wild type Lpd-PH and Lpd-RA-PH domains into the lipid monolayer. Protein was injected at the sub-phase and the change of surface pressure ( $\Delta\pi$ ) was monitored against a given initial surface pressure ( $\pi_0$ ). In general,  $\Delta\pi$  is inversely proportional to  $\pi_0$  of the phospholipid monolayer, and an extrapolation of  $\Delta\pi$  vs  $\pi_0$  yields  $\pi_c$ , which specifies an upper limit of  $\pi_0$  that a protein can penetrate. The surface pressure of cell membranes and large unilamellar vesicles has been estimated to be 31–35 dynes/cm to be able to penetrate into the cellular membranes. Thus, for a protein to effectively penetrate a particular cell membrane (or large vesicles), it should have the  $\pi_c$  value above this range for the monolayer whose lipid composition mimics that of the cell membrane. Figure 4 shows that the  $\pi_c$  values of the Lpd-PH domain for PC/PE (80:20 in mol %) and PC/PE/PI(3,4)P<sub>2</sub> (77:20:3 in mol%) lipid monolayer are 26 and 29 dynes/cm, respectively. Table 4 represents the monolayer penetration ability of the Lpd-PH domain and mutants under different lipid compositions. This  $\pi_c$  value indicates that Lpd-PH domain weakly penetrate into the lipid monolayer and this penetration ability could not be sufficient enough to penetrate into densely packed lipid bilayers or cell membranes. The inability of Lpd-PH domain to penetrate cell membrane is further supported by the kinetic SPR analysis (Figure 4). The kinetic SPR

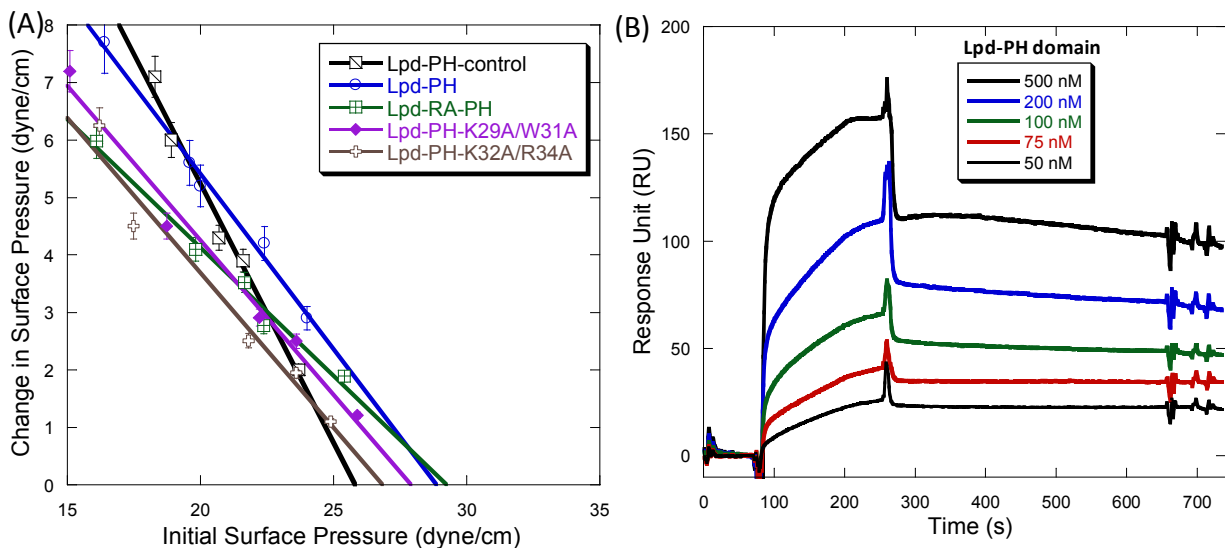
analyses indicates that the interaction of Lpd-PH domain with PI(3,4)P<sub>2</sub> containing liposome follows a two-step dissociation phases with certain conformational changes or other complex dissociation pathways.

**Table 4:** Lipid monolayer penetration properties of the Lpd-PH domain and mutants.

Protein	Lipid	$\pi_c$ values (dynes/cm)
Lpd-PH	PC/PE; (80:20)	26.0 ± 1.5
Lpd-PH	PC/PE/PI(3,4)P <sub>2</sub> ; (77:20:3)	29.3 ± 1.0
Lpd-RA-PH	PC/PE/PI(3,4)P <sub>2</sub> ; (77:20:3)	29.5 ± 1.5
Lpd-PH-K29A/W31A	PC/PE/PI(3,4)P <sub>2</sub> ; (77:20:3)	27.5 ± 0.5
Lpd-PH-K32A/R34A	PC/PE/PI(3,4)P <sub>2</sub> ; (77:20:3)	26.7 ± 0.7

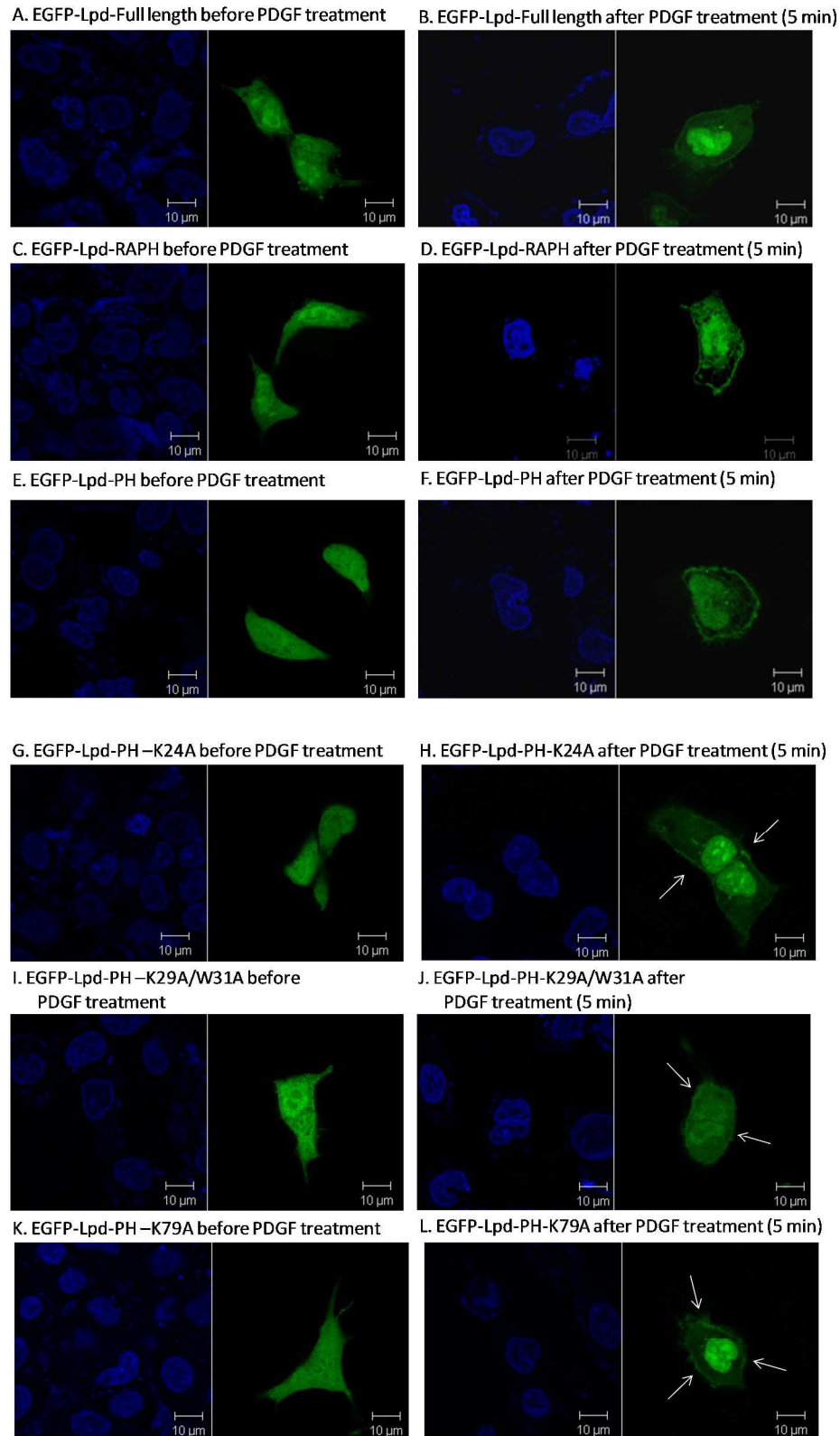
<sup>a</sup>All measurements were performed in 20 mM Tris buffer at pH 7.4 containing 160 mM NaCl.

**Cellular translocation pattern of the isolated Lpd-PH domain and mutants**— To explore the significance of PIP-dependent membrane binding properties of the PH domain and mutants under cellular environment, we monitored PDGF-mediated translocations of EGFP-fused LPD-full length, LPD-RAPH, LPD-PH and mutants in A549 cells. PDGF is reported to produce PI(3,4)P<sub>2</sub> and PI(3,4,5)P<sub>3</sub> transiently at the plasma membrane.<sup>23, 35</sup> The cells expressing similar levels of EGFP-fused PH domain/mutants were selected by visual inspections and used for PDGF-dependent translocation measurements. Serum-starvation was carried out to reduce the pre-localization of PH domain or mutants at the plasma membrane. Then the serum-starved cells were treated with 50 ng/mL of PDGF-BB and the confocal images of the fixed cells were collected (Figure 5). In general >70% of cell population showed similar behaviors with respect to membrane translocation of PH domains. Cellular images showed that a significant fraction of LPD-full length protein or LPD-RAPH and LPD-PH domain proteins translocated to the plasma membrane in a PDGF-dependent manner in A549 cells (Figure 5).



**Figure 4: Membrane penetration properties of the isolated Lpd-PH domain.** Interaction of WT-Lpd-PH domain with PC/PE/PS (60:20:20), PC/PE/PS/PI(3,4)P<sub>2</sub> (57:20:20:3) containing monolayer were measured by Langmuir trough technique (A). Kinetic SPR sensorgrams for WT-Lpd-PH interacting with PC/PE/PS/PI(3,4)P<sub>2</sub> (57:20:20:3) liposome (B). All measurements were carried out in 20 mM HEPES buffer at pH 7.4 containing 160 mM KCl at 25 °C temperature.

To further explore the significance between *in vitro* membrane binding properties of LPD-PH domain and their cellular membrane translocation, we measured the cellular localization pattern of the mutants after PDGF stimulation (Figure 5). Interestingly, the membrane translocation property of the PH-K32A/R34A mutant was almost abolished under the similar experimental conditions. However, the membrane translocation efficiencies of the other



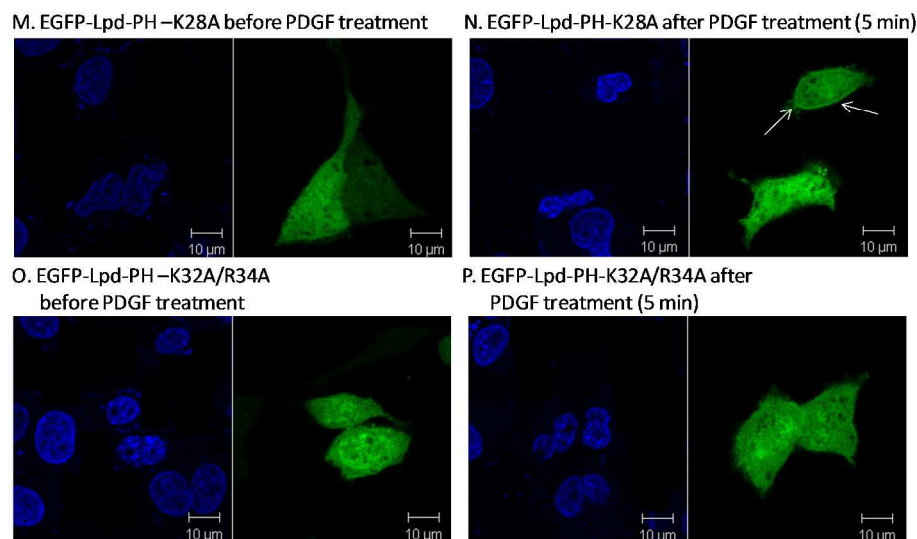


**Figure 5. Membrane translocation of EGFP-fused Lpd-PH domain and mutants in response to PDGF treatment in A549 cells.** Translocation of EGFP-fused Lpd-full length, Lpd-RAPH and Lpd-PH domain and mutants individually transfected into A549 cells were measured before (A, C, E, G, I, K, M and O) and 5 min after (B, D, F, H, J, L, N and P) the PDGF-BB treatments (50 ng/mL). Subcellular translocation patterns represents > 70% of cell populations that express similar levels of EGFP-fused Lpd-PH domain or mutants.

mutants are not that significant. Although, K29A/W31A, K79A and K28A mutants showed 3 to 7-fold differences in PI(3,4)P<sub>2</sub> binding affinities under liposomal environment, but cellular translocation patterns are not that significantly different under cellular environment. This also suggest that the PI(3,4)P<sub>2</sub>-lipid preferentially interact with the Lpd-PH domain through its canonical binding site. Overall plasma membrane translocation behaviors of the PH domain and mutants are in good agreement with our *in vitro* binding parameters.

**Table 4:** Experimental results of the PDGF-BB treated cellular translocation assay.

Protein	Cellular localization pattern after PDGF-BB treatment
EGFP-Lpd (Full length, WT)	Moderate plasma membrane translocation
EGFP-Lpd-PH (WT)	Significant plasma membrane translocation
EGFP-Lpd-RA-PH (WT)	Significant plasma membrane translocation
EGFP-Lpd-PH-K24A	Moderate plasma membrane translocation
EGFP-Lpd-PH-K29A/W31A	Moderate plasma membrane translocation
EGFP-Lpd-PH-K79A	Moderate plasma membrane translocation
EGFP-Lpd-PH-K28A	Weak plasma membrane translocation
EGFP-Lpd-PH-K32A/R34A	Predominant cytosolic distribution

## Discussion

It is well documented that PIPs divergently mediate signaling pathways in a spatially and temporally specific manner. Several studies described that most of the PIPs specifically recruits a number of effectors proteins to respective cellular membranes and play crucial role in several cellular functions.<sup>23, 24</sup> But there are insufficient studies to understand the binding nature of signaling molecules that are specifically recruited by PIPs under specific conditions. The present study describes the *in vitro* PIP-binding affinity and specificity of Lpd-PH domain and determines its significance under cellular environment. It also demonstrates the PIP-dependent membrane binding mechanism of the isolated PH domain. Our initial measurements of protein-to-membrane FRET-based competitive binding assay showed that Lpd-PH domain strongly interact with the PI(3,4)P<sub>2</sub> containing membrane. However, this PH showed only 2.7 and 5-fold weaker affinities for PI(3,4,5)P<sub>3</sub> and PI(4,5)P<sub>2</sub> lipids containing membranes, respectively. Using SPR analyses, we also found that Lpd-PH domain has significantly stronger affinity for PI(3,4)P<sub>2</sub> containing liposomes. Both equilibrium- and kinetic-SPR analyses showed that PI(3,4)P<sub>2</sub> binding affinities are 3 to 5-fold stronger than PI(3,4,5)P<sub>3</sub> and PI(4,5)P<sub>2</sub> lipids under the similar experimental conditions. This binding preference for PI(3,4)P<sub>2</sub> lipid could be due to the proper fitting of the headgroup into the cationic groove with preferential interactions for D3- and D4-

phosphate groups of the myo-inositol ring. In order to understand the significance of this *in vitro* PI(3,4)P<sub>2</sub> lipid binding preference, we performed cellular translocation studies of the EGFP-fused Lpd-full length, Lpd-RA-PH and Lpd-PH domain proteins in A549 cells in the absence and presence of PDGF. Confocal measurements clearly showed that EGFP-fused Lpd-PH domain predominantly translocated to the plasma membrane of the A549 cells upon stimulation with PDGF. PDGF is known to transiently produce PI(3,4)P<sub>2</sub>/PI(3,4,5)P<sub>3</sub> at the plasma membrane. This supports our binding parameters measured by both FRET and SPR analyses.<sup>23, 35</sup>

For further understanding of the PI(3,4)P<sub>2</sub> binding mechanism of the Lpd-PH domain mutational analysis of the cationic residues were performed. Homology sequence alignment and the reported crystal structure (PDB code: 4GN1) identified that K24, K28, K29, K32, R34, K79, and K96 cationic residues could be the probable PIP-binding residues of Lpd-PH domain.<sup>6</sup> However, further detailed analysis of Lpd-PH domain crystal structure revealed that K28, K32 and K34 forms a canonical PIP-binding site of the PH domain, whereas K24, K29, K79 and K96 residues constitute a non-canonical PIP-binding site for the Lpd-PH domain like that of  $\beta$ -spectrin protein.<sup>27</sup> Our molecular docking analyses with short chain (n = 4) PI(3,4)P<sub>2</sub> and Ins(1,3,4)P<sub>3</sub> showed that the PH domain can interact with both the cationic grooves. Mutational studies of the cationic residues showed their significant role in PIP-dependent membrane interactions. Kinetics-SPR based binding affinity calculation showed that K32A/R34A mutation showed over 25-fold binding affinity difference where as K28A mutation showed ~5-fold binding affinity difference with the WT-Lpd-PH domain for PI(3,4)P<sub>2</sub> lipid binding. Whereas other mutants showed only 2-7-fold binding affinity difference for PI(3,4)P<sub>2</sub> lipids. This clearly suggests that K32/R34 preferentially interact with the headgroup of PI(3,4)P<sub>2</sub> lipid. Based on our molecular docking results we presume that D3-phosphate and D4-phosphate preferentially

interacts with K32 and R34 whereas K28 could be responsible for its interaction with D1-phosphate of the PI(3,4)P<sub>2</sub> lipid. Membrane translocation studies with the mutants showed that the double mutant K32A/R34A predominantly localize at the cytoplasm in the PDGF stimulated A549 cells. The other mutants showed partial membrane localization under the similar experimental conditions.

Another significant observation from our PIP-dependent membrane binding studies is the partial membrane penetration of the Lpd-PH domain in a PI(3,4)P<sub>2</sub>-dependent manner. Although our monolayer penetration measurements shows that the monolayer penetration ability of the Lpd-PH domain get enhanced in the presence of PI(3,4)P<sub>2</sub> lipid, but the extent of penetration might not be significant enough to penetrate biological membranes. It is reported that only few PH domain like DAPP1-PH domain could penetrate into the biological membrane significantly.<sup>23</sup> Therefore, membrane interaction of Lpd-PH domain takes place primarily due to specific interactions with the headgroup of PI(3,4)P<sub>2</sub> lipid.

It is important to mention that there is some considerable discrepancy between our *in vitro* PIP-binding affinity data and reported data. Recently, Professor Jinhua Wu and coworkers determined the PIP-binding specificity and affinity of Lpd-cc-RA-PH domain using fluorescent polarization (FP) assay and found no specificity.<sup>3, 6</sup> But our biophysical studies suggest that isolated Lpd-PH domain strongly interacts with PI(3,4)P<sub>2</sub> lipid which is in accordance with previously reported PIP-binding specificity measured by protein-lipid overlay assay.<sup>3</sup> Professor Frank B. Gertler and coworkers also showed that Lpd-PH domain localize at the ruffles in PDGF-stimulated Rat2 fibroblasts.<sup>3</sup> Very often this kind of discrepancy arises due to the binding parameters measured using different experimental design (e.g fluorometric, lipid dot blot, vesicle-pelleting, SPR and others) and conditions. Therefore, it is difficult to directly compare

with reported affinities data. Our quantitative measurements of binding affinities and cellular localization studies are well correlated and were measured thoroughly and systematically. Our *in vitro* binding studies showed that Lpd-PH domain preferentially interact with the PI(3,4)P<sub>2</sub> lipid, over other PI3-kinase products like PI(3,4,5)P<sub>3</sub> and PI(3)P lipids. However, both FRET and SPR analyses showed that PI(3,4)P<sub>2</sub> had only ~3-fold stronger binding preference over PI(3,4,5)P<sub>3</sub> lipid. PDGF is also reported to produce both (3,4)P<sub>2</sub> and PI(3,4,5)P<sub>3</sub> lipid at the plasma membrane.<sup>23, 35</sup> Therefore, in addition to PI(3,4)P<sub>2</sub>, PI(3,4,5)P<sub>3</sub> can also assist in membrane translocation of Lpd protein under different cellular conditions.

## Conclusion

Taken together all results in the present study establishes that Lpd-PH domain strongly interacts with PI(3,4)P<sub>2</sub> lipid containing membrane without membrane penetration and is sufficient for membrane localization. *In vitro* binding studies systematically determined the PIP-specificity of the PH domain for PI(3,4)P<sub>2</sub> over other lipids. Mutational based PIP-binding affinity and specificity measurements demonstrate detail membrane docking properties of Lpd-PH domain. Our *in vitro* binding measurements are in good correlation with the cellular localization of the isolated Lpd-PH domain. This indicates that the kinetics of PI-mediated cellular membrane recruitment of this PH domain is governed, to a large extent, by their membrane binding properties. This would also help in account for different cellular functions and regulation of this protein. Furthermore, our results should form the foundation of systematic and quantitative assessment of different cellular membrane translocation properties of a large number of PH domains and their host proteins.

## Experimental Procedures

**Materials**— Phosphatidylinositol-3,4-bisphosphate (PtdIns(3,4)P<sub>2</sub>), phosphatidylinositol-4,5-bisphosphate (PtdIns(4,5)P<sub>2</sub>), and phosphatidylinositol-3,4,5-triphosphate (PtdIns(3,4,5)P<sub>3</sub>), phosphatidylinositol-3-phosphate(PtdIns(3)P), phosphatidylinositol-4-phosphate(PtdIns(4)P), phosphatidylinositol-5-phosphate(PtdIns(5)P), phosphatidylinositol were purchased from Cayman Chemicals. 1-Palmitoyl-2-oleoyl-*sn*-glycero-3-phosphocholine (POPC), 1-palmitoyl-2-oleoyl-*sn*-glycero-3-phosphoethanolamine (POPE), and 1-palmitoyl-2-oleoyl-*sn*-glycero-3-phosphoserine (POPS) were purchased from Avanti Polar Lipids. Octyl glucoside was purchased from Fisher. The Pioneer L1 sensor chip was purchased from GE Healthcare.

**Vector construction and mutagenesis**— For bacterial expression, the cDNA of Lpd-PH , Lpd-RA-PH, Lpd-PH domain mutants, W22A, D25G/ L23R, D25G/L23R/K29A, K29A/ W31A, K79A, K24A, K32A/ R34A, K28A/K29A/K96A were subcloned into the vector pGEX-6P-1 between the *EcoRI* and *BamHI* restriction sites with N-terminal glutathione S-transferase (GST) fusion. The cDNA of full length Lpd-PH-EGFP and Lpd-RAPH-EGFP were the kind gift from Professor Matthias Krause (King's College London). Lpd-PH domain mutants were generated by the overlap extension PCR and subcloned into pEGFP-N1 vector between the *KpnI* and *XhoI* restriction sites with N-terminus enhanced green fluorescence protein (EGFP). All constructs were transformed into DH5 $\alpha$  cells for plasmid isolation. All plasmid DNA sequences were verified. All GST constructs were transformed into E. coli BL21 (DE3) cells for protein expression.

**Protein expression and purification**— The pGEX-6P1 constructs encoding the PH domain and mutants were transformed into BL21(DE3) E.coli and bacteria was grown at 37 °C in 1lit Luria broth medium containing 100µg/ml ampiciline until the optical density was ~0.7 at 600 nm. To induce the cells 500 µM isopropyl-D-thiogalactoside (IPTG) was added and kept for 16 hrs at 24 °C, 120 rpm continuous shaking. After that cells were pelleted down and resuspension in 20ml 20 mM Tris-buffer, pH-8 containing 160 mM NaCl, 1% TritonX-100, 1mM DTT and 0.5 mM PMSF. Resultant solution was completely lysed by probe sonicator and was centrifuged at 20,000 rpm, for 40 minutes at 4 °C. Supernatant was collected and 200 µl glutathione-sepharose resin was added to the solution and was equilibrated for 30 min in 60 rpm on a shaker.

**FRET measurements**— The FRET based liposome binding affinities of Peripheral proteins are well established through lipid binding domains at the plasma membrane. The PH domain of Lpd has also similar property. To measure the binding affinity of PH domain of Lpd, we successfully performed protein to membrane FRET assay and competitive binding assay.<sup>25</sup> PIPs lipids used as ligand to prepare liposome. The FRET signal monitored with and without ligand for subsequent background correction where Tryptophan residue of PH domain acts as FRET donor and dansyl-PE acts as FRET acceptors. We successfully studied FRET competitive binding assay for the binding affinity and specificity of Lpd-PH domain to the PIP lipid containing membrane. We used IP<sub>6</sub> as competitive inhibitor of PH domain to displace the protein from targeted ligand containing membrane and calculating the apparent inhibitory constant [ $K_I(IP_6)_{app}$ ].

**SPR measurements**— To measure the PH domain binding affinity and specificity to the PIs we performed a real time SPR measurement as reported in various studies, at 25°C temperature.

Lipid-coated L1 sensor chip was used in the Biacore X100 (GE Healthcare).<sup>23,36</sup> All studies were carried out using 20 mM Tris, 160 mM KCl, pH-7.4, running buffer, POPC/POPE(80:20), POPC/POPE/PI<sub>x</sub> (77:20:3) containing vesicles at the flow rate of 5 $\mu$ l/min to the control and active surface respectively. 4500 response units of PI(3,4)P2 containing vesicles were coated to the active surface or flow cell-2 and PI(3,4)P2 free vesicles were coated to the control surface or flow cell-1 as control to monitor subsequent nonspecific binding. For kinetic SPR measurements, the sensorgrams were obtained using six different concentration of each protein within a 10-fold range of dissociation constant ( $K_d$ ). The  $K_d$  is mainly determined by equilibrium SPR measurements. The association ( $k_{on}$ ) and dissociation ( $k_{off}$ ) rate constants can be determined from the sensorgrams using a curve fit algorithm. The equilibrium dissociation constant also can be calculated from the ratio of rate constants assuming a simple one-step (protein + vesicle  $\leftrightarrow$  [protein·vesicle]) or two-step (protein + vesicle  $\leftrightarrow$  [vesicle/protein]  $\leftrightarrow$  [protein\*·vesicle]) models.

***Monolayer penetration measurement***— Lipid monolayer at the air-water interface have been widely used for studying membrane-protein interactions, because the surface packing density of the lipids can readily and accurately varied in the system. Studies have shown that monolayer and bilayer have many common physical properties and that information about one state can be translated to other. The lipid monolayer system is particularly useful for measuring membrane-penetrating activities of proteins in terms of change in surface pressure ( $\Delta\pi$ ) at constant surface area or change in surface area at constant surface pressure. The measured  $\Delta\pi$  is in general proportional to the initial surface pressure ( $\pi_0$ ) of the lipid monolayer and an extrapolation of the  $\Delta\pi$  versus  $\pi_0$  plot yields critical surface pressure ( $\pi_c$ ) which specifies the upper limit of  $\pi_0$  that the protein can penetrate into. The surface pressure of the cell membranes has been estimated to be

31-35 dyne/cm. The recent studies on many lipid binding proteins have shown that those proteins whose physiological action involved penetration into particular cell membrane can penetrate the cell membrane mimicking monolayer with  $\pi_c > 31$  dyne/cm.<sup>23, 24</sup> Biological membrane penetration of Lpd-PH domain investigated by measuring a change in the surface pressure ( $\pi$ ) into the phospholipid monolayers of different lipid composition. The experiment was carried out using 10 mM Tris, 160 mM NaCl at pH-7.4 buffer, a 10 ml Teflon trough and a Wilhelmy plate connected to a Cahn microbalance as reported previously.<sup>23</sup> We monitored the surface pressure change ( $\Delta\pi$ ) of lipid monolayer after addition of 10  $\mu$ g protein through a hole in the wall of the trough. After 30 min, surface pressure reached maximum and critical surface pressure ( $\pi_c$ ) determined, plotting the change of surface pressure ( $\Delta\pi$ ) versus initial surface pressure ( $\pi_0$ ).

***Cellular translocation measurements***— Membrane localization of PH domain and its host protein were monitored by expressing the EGFP fused Lpd in human PDGF-BB stimulated non-small cell lung cancer A549 cells.<sup>23</sup> Cells were cultured into six wells of a sterile Nunc Lak-TekII<sup>TM</sup> chambered cover glass plate containing Dulbecco's modified Eagle's medium (DMEM) and 10% fetal bovine serum, incubated at 37 °C with 5% CO<sub>2</sub> for 24 h. The cells were transiently transfected with appropriate expression plasmid using lipofectamine. Before the treatment of PDGF-BB transfected cells were starved with serum free medium for 10 hours. Then media was replaced with fresh serum free medium followed by addition of human PDGF-BB (50 ng/mL) and incubated for 5 minutes. Then cells were fixed and prepared for imaging study. Before confocal imaging all transfected cells were washed three times with phosphate-buffered saline (PBS) and then fixed by using 4% paraformaldehyde at room temperature for 15 min. Then cells were permeabilized with 0.1% Triton X-100 for 10 min. The permeabilized cells were again

washed three times with PBS and then coverslips were mounted with mounting media containing DAPI (Santa cruz mounting medium) on a glass slide (Blue star). The subcellular localization of the proteins were observed with a Zeiss LSM 510 confocal microscope with an Axiovert 100 M inverted microscope operating with a 25 milliwatt argon laser tuned to 488 nm.

**Molecular docking analysis**— Molecular docking was performed using the model structure of LPD-PH domain using Modeller 9v7. The model structure was generated using the crystal structure of LPD-RAPH domain (Protein Data Bank code: 4GN1).<sup>6</sup> The energy minimized three-dimensional structure of ligands was prepared by using the GlycoBioChem PRODRG2 Server (<http://davapc1.bioch.dundee.ac.uk/prodrg/>). The GRONingen MACHine for Chemical Simulations (GROMACS) library of three-atom combination geometries employing a combination of short molecular dynamics simulations and energy minimizations was utilized for the conversion of 2D molecular structures to 3D structures. Ligand-protein docking was performed with using the Molegro Virtual Docker software, version 4.3.0 (Molegro ApS, Aarhus, Denmark). The binding site was automatically detected by the docking software and restricted within spheres with radius of 15 Å. During virtual screening, the following parameters were fixed: number of runs 10, population size 50, crossover rate 0.9, scaling factor 0.5, maximum iteration 2,000 and grid resolution 0.30. The docked results were evaluated on the basis of moledock and re-rank score. The poses were exported and examined with *PyMOL* software.

## Acknowledgements

The authors are also thankful to the BRNS (2009/20/37/5/BRNS/3331) Govt. of India for financial support. The authors acknowledge their sincere gratitude to the Department of Chemistry, Centre for the Environment, DBT Programme Support (no. BT/01/NE/PS/08), Indian Institute of Technology Guwahati, India for instrument supports. Special thanks are due to Dr Priyadarshi Satpati for his helpful suggestions.

**Electronic supplementary information (ESI) available:** Surface plasmon resonance sensorgrams, binding parameter of the Lpd-PH domain and MD simulation method and results.

## References

1. G. P. Colo, E. M. Lafuente and J. Teixido, *Eur. J. Cell Biol.*, 2012, **91**, 861-868.
2. M. Krause, E. W. Dent, J. E. Bear, J. J. Loureiro and F. B. Gertler, *Annu. Rev. Cell Dev. Biol.*, 2003, **19**, 541-564.
3. M. Krause, J. D. Leslie, M. Stewart, E. M. Lafuente, F. Valderrama, R. Jagannathan, G. A. Strasser, D. A. Rubinson, H. Liu, M. Way, M. B. Yaffe, V. A. Boussiotis and F. B. Gertler, *Dev. Cell*, 2004, **7**, 571-583.
4. E. M. Lafuente, A. A. van Puijenbroek, M. Krause, C. V. Carman, G. J. Freeman, A. Berezovskaya, E. Constantine, T. A. Springer, F. B. Gertler and V. A. Boussiotis, *Dev. Cell*, 2004, **7**, 585-595.
5. G. Tasaka, M. Negishi and I. Oinuma, *J. Neurosci.*, 2012, **32**, 8293-8305.
6. Y. C. Chang, H. Zhang, M. L. Brennan and J. Wu, *Protein Cell*, 2013, **4**, 211-219.
7. R. S. Depetris, J. Wu and S. R. Hubbard, *Nat. Struct. Mol. Biol.*, 2009, **16**, 833-839.
8. P. Rodriguez-Viciano, C. Sabatier and F. McCormick, *Mol. Cell Biol.*, 2004, **24**, 4943-4954.
9. J. P. Wynne, J. Wu, W. Su, A. Mor, N. Patsoukis, V. A. Boussiotis, S. R. Hubbard and M. R. Philips, *J. Cell Biol.*, 2012, **199**, 317-330.
10. M. Geese, J. J. Loureiro, J. E. Bear, J. Wehland, F. B. Gertler and A. S. Sechi, *Mol. Biol. Cell*, 2002, **13**, 2383-2396.
11. S. Dowler, R. A. Currie, D. G. Campbell, M. Deak, G. Kular, C. P. Downes and D. R. Alessi, *Biochem. J.*, 2000, **351**, 19-31.
12. J. E. Bear, T. M. Svitkina, M. Krause, D. A. Schafer, J. J. Loureiro, G. A. Strasser, I. V. Maly, O. Y. Chaga, J. A. Cooper, G. G. Borisy and F. B. Gertler, *Cell*, 2002, **109**, 509-521.
13. K. Niebuhr, F. Ebel, R. Frank, M. Reinhard, E. Domann, U. D. Carl, U. Walter, F. B. Gertler, J. Wehland and T. Chakraborty, *EMBO J.*, 1997, **16**, 5433-5444.
14. K. Rottner, B. Behrendt, J. V. Small and J. Wehland, *Nat. Cell Biol.*, 1999, **1**, 321-322.

15. F. B. Gertler, K. Niebuhr, M. Reinhard, J. Wehland and P. Soriano, *Cell*, 1996, **87**, 227-239.
16. B. Drees, E. Friederich, J. Fradelizi, D. Louvard, M. C. Beckerle and R. M. Golsteyn, *J. Biol. Chem.*, 2000, **275**, 22503-22511.
17. S. Gruenheid and B. B. Finlay, *Nature*, 2003, **422**, 775-781.
18. F. Frischknecht and M. Way, *Trends Cell Biol.*, 2001, **11**, 30-38.
19. H. Li, L. M. Schopfer, P. Masson and O. Lockridge, *Biochem J.*, 2008, **411**, 425-432.
20. L. E. Rameh and L. C. Cantley, *J. Biol. Chem.*, 1999, **274**, 8347-8350.
21. G. Di Paolo and P. De Camilli, *Nature*, 2006, **443**, 651-657.
22. J. M. Kavran, D. E. Klein, A. Lee, M. Falasca, S. J. Isakoff, E. Y. Skolnik and M. A. Lemmon, *J. Biol. Chem.*, 1998, **273**, 30497-30508.
23. D. Manna, A. Albanese, W. S. Park and W. Cho, *J. Biol. Chem.*, 2007, **282**, 32093-32105.
24. W. Cho and R. V. Stahelin, *Annu. Rev. Biophys. Biomol. Struct.*, 2005, **34**, 119-151.
25. N. Mamidi, R. Borah, N. Sinha, C. Jana and D. Manna, *J. Phys. Chem. B*, 2012, **116**, 10684-10692.
26. D. Manna, N. Bhardwaj, M. S. Vora, R. V. Stahelin, H. Lu and W. Cho, *J. Biol. Chem.*, 2008, **283**, 26047-26058.
27. M. Hyvonen, M. J. Macias, M. Nilges, H. Oschkinat, M. Saraste and M. Wilmanns, *EMBO J.*, 1995, **14**, 4676-4685.
28. S. Tuzi, N. Uekama, M. Okada, S. Yamaguchi, H. Saito and H. Yagisawa, *J. Biol. Chem.*, 2003, **278**, 28019-28025.
29. F. M. Flesch, J. W. Yu, M. A. Lemmon and K. N. Burger, *Biochem. J.*, 2005, **389**, 435-441.
30. W. Cho, L. Bittova and R. V. Stahelin, *Anal. Biochem.*, 2001, **296**, 153-161.
31. W. A. Kimber, L. Trinkle-Mulcahy, P. C. Cheung, M. Deak, L. J. Marsden, A. Kieloch, S. Watt, R. T. Javier, A. Gray, C. P. Downes, J. M. Lucocq and D. R. Alessi, *Biochem. J.*, 2002, **361**, 525-536.
32. B. Ananthanarayanan, S. Das, S. G. Rhee, D. Murray and W. Cho, *J. Biol. Chem.*, 2002, **277**, 3568-3575.
33. H. Yagisawa, K. Sakuma, H. F. Paterson, R. Cheung, V. Allen, H. Hirata, Y. Watanabe, M. Hirata, R. L. Williams and M. Katan, *J. Biol. Chem.*, 1998, **273**, 417-424.
34. L. J. Holt and R. J. Daly, *Growth Factors*, 2005, **23**, 193-201.
35. Y. Artemenko, A. Gagnon, S. Ibrahim and A. Sorisky, *J. Cell Physiol.*, 2007, **211**, 598-607.
36. N. Mamidi, S. Panda, R. Borah and D. Manna, *Mol. Biosyst.*, 2014, **10**, 3002-3013.